Nonlinear Dyn (2019) 98:3143–3153
https://doi.org/10.1007/s11071-019-05128-w

ORIGINAL PAPER

Fractional-order model and experimental verification for broadband hysteresis in piezoelectric actuators

Changshun Ding · Junyi Cao · YangQuan Chen

Received: 20 December 2018 / Accepted: 10 July 2019 / Published online: 18 July 2019

Abstract Piezoelectric actuators are increasingly popular for high-accuracy and high-speed nanopositioning systems. However, nonlinear rate-dependent hysteresis of piezoelectric actuators leads to many difficulties in accurately analyzing the dynamic characteristics of piezoelectric nanopositioning systems in a wide frequency band. This paper proposes fractional-order model methods to characterize the hysteresis of piezoelectric actuators in time and frequency domains. Input voltage and output displacement of the piezoelectric actuator in time domain are employed to identify the parameters of the fractional-order model. Moreover, amplitude and phase errors are utilized to obtain the fractional model in frequency domain. Simulations and experiments are performed to validate the effectiveness of the proposed fractional-order model. The results show that the identified model in frequency domain is preferable in a wider frequency range from 1 to 200 Hz, and the maximum error is about 4.47%.

Keywords Fractional-order model · Piezoelectric actuators · Hysteresis nonlinearity · Broadband

C. Ding · J. Cao (✉)
Key Laboratory of Education Ministry for Modern Design and Rotor-Bearing System, School of Mechanical Engineering, Xi'an Jiaotong University, Xi'an 710049, China
e-mail: caojy@mail.xjtu.edu.cn

Y. Chen
School of Engineering, University of California, Merced 95343, USA
e-mail: ychen53@ucmerced.edu

1 Introduction

High-accuracy and high-speed nanopositioning systems have a wide range of applications in many significant occasions, such as atomic force microscopes and micromanipulations. The traditional motor-driven approach has some drawbacks and could not meet the high performance demands of nanopositioning systems. Piezoelectric actuators have been widely employed as the actuating element of high-speed nanopositioning systems due to its high resolution, fast response and large output force [1–5]. However, there is a nonlinear output response due to the intrinsic hysteresis when the excitation voltage is applied to piezoelectric actuators. Moreover, the nonlinear hysteresis may usually lead to undesirable inaccuracies and system instability. Generally, the hysteresis is described by the multi-valued nonlinear function with the input and output of the system. It also has great dependence of frequency and amplitude of input signals. The previous investigations showed that there will be almost 15% error caused by the hysteresis, and it can not be ignored in the precise positioning [6]. Therefore, it is very significant to accurately analyze and control the dynamic characteristics of piezoelectric nanopositioning systems in a wider frequency bandwidth [7]. The precise modeling of nonlinear rate-dependent hysteresis of piezoelectric actuators still attract the considerable interest of many researchers in the multidiscipline field [8].

In order to improve the control precision of piezoelectric actuators, many efforts had been made to develop nonlinear hysteresis models for characterizing nonlinear phenomenon of piezoelectric actuators, such as Preisach model [9–11], Prandtl–Ishlinskii model and its modification [12–16], Maxwell model [17–19], and Bouc–Wen model [20–22]. These models were employed by multidisciplinary researchers for describing the rate-dependent characteristics of hysteresis. However, it is very complicated to perform the double integral calculation process for the Preisach model and identify key parameters of Prandtl–Ishlinskii model and the Bouc–Wen model. More importantly, great effort has been dedicated to improve the control performance under a constant frequency or relative narrow frequency bandwidth in recent years. However, the mathematical model of piezoelectric ceramic actuators under broadband frequency environments is required to be further investigated to meet the broadband demand in the real engineering.

Fractional calculus theory is a generalization of the conventional integration and differentiation to non-integer orders. Recently, various complex systems are successfully described by fractional calculus due to its advantageous frequency-dependent characteristics. In particular, there are many successful applications in the field of mechanical constitutive relations of complex viscoelastic materials and system control, highlighting its own unique advantages, irreplaceability, and theoretical completeness [23–29]. Zakeri et al. [30] proposed a novel interval type-2 fuzzy fractional-order super-twisting algorithm and demonstrated its effectiveness in fully actuated and under-actuated systems. Zolotas et al. [31] investigated the fractional-order controlling of railway vehicle suspensions and achieved 7.5–25% improvement in ride quality under the same maximum suspension deflection. The fractional-order model also has been used to describe the hysteresis nonlinearity of piezoelectric actuators in the specific frequency. Rebai et al. [32] proposed an approach to identify fractional-order models, and their numerical simulations show that the fractional-order model can better describe the hysteresis nonlinearity of piezoelectric actuators in comparison with an integer-order model during the excitation frequency of 50 Hz. Li et al. [33] introduced a fractional-order operator to the control system for piezo-actuated nanopositioning stages, and their results show that in spite of incomprehensive understanding of the fractional characteristics of piezoelectric actuators, the fractional-order control approach improved the bandwidth of the nanopositioning stages. Liu et al. [34] integrated fractional-order dynamics into the Maxwell resistive capacitor model to describe the effect of hysteresis, and experimental results showed the robustness to the amplitude change of the input voltage in the case of constant frequency. Obviously, previous models with fractional calculus were successfully applied for describing the nonlinearity of piezoelectric actuators in some specific frequencies. However, the broadband motion demand of piezoelectric actuators is popular in the field of vibration control and micro-scanning measurements. There are few investigations into the dynamic model of broadband hysteresis of piezoelectric systems in the past decade. Therefore, this paper will numerically and experimentally investigate different fractional-order model methods to describe the hysteresis of piezoelectric actuators in a wider frequency bandwidth.

In this paper, fractional-order models are proposed to describe the hysteresis of a piezoelectric actuator. A type of Laplace transform of the fractional-order linear differential equation is chosen as the fractional-order model. The fractional-order model is utilized to describe the relationship between the input voltage and the output displacement of a piezoelectric actuator. Then an identified approach is developed to identify the parameters of the fractional-order model from input voltage and output displacement of the piezoelectric actuator in time domain. Moreover, amplitude and phase values in frequency domain are employed to identify the frequency model for further improving the model accuracy in a wider bandwidth. Validation and performances evaluation of the proposed approach are carried out with simulation and experiments.

This paper is organized as follows: an introduction to fractional-order calculus is given in Sect. 2. Then in Sect. 3, the fractional-order model of hysteresis is discussed in more details and its parameters are identified in time domain. And in Sect. 4, the fractional-order model is identified with the amplitude and phase values in frequency domain. Conclusions are followed in Sect. 5.

2 Fractional-order systems

Fractional calculus is a generalization of integration and differentiation to non-integer order, with the oper-

ator ${}_{t_0}D_t^{\alpha}$, where t_0 and t are the lower boundary and upper boundary of integration, respectively, and α is the fractional order, and it can be a complex number. In general, the operator ${}_{t_0}D_t^{\alpha}$ is defined as follows [23]:

$$ {}_{t_0}D_t^{\alpha} = \begin{cases} \frac{\mathrm{d}^{\alpha}}{\mathrm{d}t^{\alpha}}, & \mathrm{Re}(\alpha) > 0 \\ 1, & \mathrm{Re}(\alpha) = 0 \\ \int_0 (\mathrm{d}\tau)^{-\alpha}, & \mathrm{Re}(\alpha) < 0 \end{cases} \tag{1} $$

where $\mathrm{Re}(\alpha)$ is the real part of α.

There are kinds of definitions of the explanation of fractional order operator, such as Grunwald–Letnikov (G–L) definition and Riemann–Liouville (R–L) definition. The R–L definition is a common one, which is shown as follows [23]:

$$ {}_{t_0}D_t^{\alpha} f(t) = \frac{1}{\Gamma(m-\alpha)} \left(\frac{\mathrm{d}}{\mathrm{d}t}\right)^m \times \int_{t_0}^{t} \frac{f(\tau)}{(t-\tau)^{1-(m-\alpha)}} \mathrm{d}\tau, \; m-1 < \alpha < m \tag{2} $$

where $\Gamma(.)$ is the well-known Euler's gamma function.

In this paper, the approximate calculation of G–L definition is employed to carry out the numerical simulation of fractional-order operators, and the G–L definition is given as [23]:

$$ {}_{t_0}D_t^{\alpha} f(t) = \lim_{h\to 0} h^{-\alpha} \times \sum_{j=0}^{[(t-t_0/h)]} (-1)^j \frac{\Gamma(\alpha+1)}{\Gamma(\alpha-j+1)\Gamma(j+1)} f(t-jh) \tag{3} $$

where $\Gamma(.)$ is the well-known Euler's gamma function; h is the calculation step; n is an integer.

Fractional-order systems can be represented by a fractional-order linear differential equation of the form:

$$ a_0 D^{\alpha_0} y(t) + \cdots + a_n D^{\alpha_n} y(t) = b_0 D^{\beta_0} u(t) + \cdots + b_m D^{\beta_m} u(t) \tag{4} $$

where $u(t)$ and $y(t)$ are, respectively, the system input and output. $D^{\alpha} y(t)$ is the α time derivative of $y(t)$.

If Laplace transform of $D^{\alpha} x(t)$with zero initial condition:

$$ L\{D^{\alpha} x(t)\} = s^{\alpha} X(s) \tag{5} $$

Then, taking Laplace transform of the two sides in Eq. (4), the fractional-order linear time-invariant (LTI) system can be described by the following transfer function:

$$ G(s) = \frac{Y(s)}{U(s)} = \frac{b_0 s^{\beta_0} + \cdots + b_m s^{\beta_m}}{a_0 s^{\alpha_0} + \cdots + a_n s^{\alpha_n}} \tag{6} $$

with $\alpha_0 < \alpha_1 < \cdots < \alpha_n$ and $\beta_0 < \beta_1 < \cdots < \beta_m$.

To take advantage of the memory effects of fractional-order operations, the nonlocal memory-dominant nature of hysteresis could be well described and the hysteresis would be suitable to be described as a fractional-order model.

In Sects. 3 and 4, different fractional-order models will be proposed to describe the hysteresis of the piezoelectric actuator.

3 Hysteresis identification in time domain

In this section, the routine for parameter identification in the time domain is given, including modeling, parameter identification, and optimization. The experimental verification is carried out.

3.1 Hysteresis modeling

To develop the fractional-order hysteresis model for a piezoelectric actuator, it is necessary to study the feature of the hysteresis existing in the piezoelectric actuators. Hysteresis of the piezoelectric actuators is frequency-dependent and amplitude-dependent. The characteristics of hysteresis will change when the frequency and amplitude of the input signals change. Several hysteresis loops under input sinusoidal signals with different frequencies are shown in Fig. 1. Results show that the hysteresis error will enlarge as the frequency of input signal increases and the peak-to-peak amplitude will decrease as the frequency of input signal increases.

Figure 2a shows the PZT actuator used for experimental verification in this paper. It consists of an integration machine design structure of piezoelectric stack and flexible hinge. The combined mechanism can be equivalent to a damped mass-spring system shown in Fig. 2b. Therefore, based on Newton's second law of motion, the governing differential equation of the piezoelectric actuator can be expressed as:

$$ m\ddot{x}(t) + (c_p + c)\dot{x}(t) + (k_p + k)x(t) = F_p(t) \tag{7} $$

where m is the equivalent mass of the piezoelectric actuator; x(t) is the output displacement of the piezoelectric actuator; c and c_p are, respectively, damping

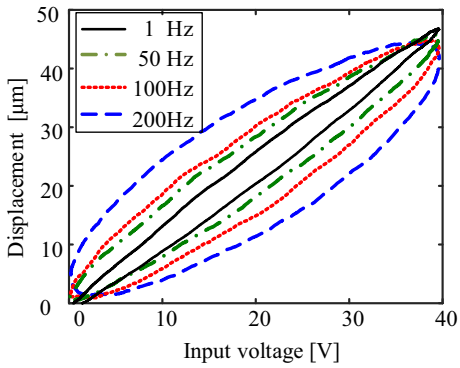

Fig. 1 Hysteresis loops with the different frequencies

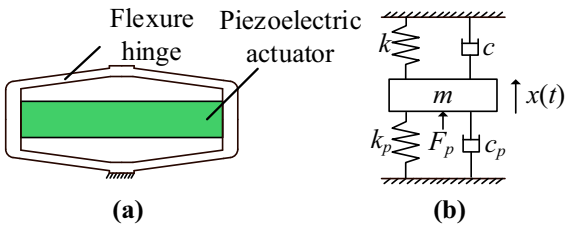

Fig. 2 The equivalent dynamic model of the piezoelectric actuator: **a** schematic diagram of piezoelectric actuator; **b** the equivalent dynamics model

coefficients of the flexible hinge and the piezoelectric stack; k and k_p are, respectively, the equivalent stiffness of the flexible hinge and the piezoelectric stack; $F_p(t)$ is the driving force of the piezoelectric stack, which can be expressed as:

$$F_p(t) = nd_{33}k_pU_p(t) \tag{8}$$

where n is the number of layer in the piezoelectric stack; d_{33} is the piezoelectric constant; $U_p(t)$ is the voltage applied to the piezoelectric stack. Equation (8) is based on the linear assumption, but the nonlinear hysteresis effects cannot be ignored. To describe the hysteresis nonlinearity between actual voltages applied to the piezoelectric stack and the corresponding displacements of the piezoelectric actuator, a hysteresis force model can be described by a linear fractional-order differential equation, which can be given as:

$$F_p(t) + aD^{\lambda}F_p(t) = nd_{33}kpU_p(t) + bD^{\delta}U_p(t) \tag{9}$$

where λ and δ are, respectively, the differential orders of the driving force and the applied voltage; a and b are constant gains.

Taking Laplace transform of two sides in Eqs. (7) and (9), the transfer function of the piezoelectric actuator system is obtained as:

$$\begin{aligned} G(s) &= \frac{X(s)}{U(s)} \\ &= \frac{nd_{33}k_p + bs^{\delta}}{1 + as^{\lambda}} \cdot \frac{1}{ms^2 + (c + c_p)s + (k + k_p)} \end{aligned} \tag{10}$$

where s denotes the Laplace operator; $X(s)$ and $U(s)$ denote the Laplace transform of $x(t)$ and $U_p(t)$, respectively.

In order to make the identification process more simple, Eq. (10) can be simplified to the fractional-order model of piezoelectric actuators with 10 parameters:

$$G(s) = \frac{a_5s^{a_{10}} + a_6}{a_1s^{a_7} + a_2s^{a_8} + a_3s^{a_9} + a_4} \tag{11}$$

3.2 Experiment setup

The experimental system shown in Fig. 3 is set up to obtain the input and output response for identifying the model parameters in Eq. (11). The displacement of a piezoelectric actuator (model P06.X150AK from coremorrow S&T Co., Ltd) is 175 μm under 150V input signal voltage. The excitation signal of the piezoelectric actuator is generated by the signal generator (model AFG310 from Sony-Tektronix) and amplified by a power amplifier (model M5041 from PI) with a fixed gain of 10 and a bandwidth of 1000 Hz. The displacement of the PZT actuator is measured by a laser displacement sensor (model ILD2200-2 from Micro-epsilon). The input voltage and output displacement are acquired and stored by the oscilloscope (model MSOX3050A from Agilent). All the above instruments are installed on the vibration-isolated platform to reduce external disturbances.

3.3 Parameter identification and optimization

The sinusoidal signal is employed to be the input signal for the identification. The data of sinusoidal input voltage and output displacement response are recorded under different frequencies ranging from 1 to 200 Hz.

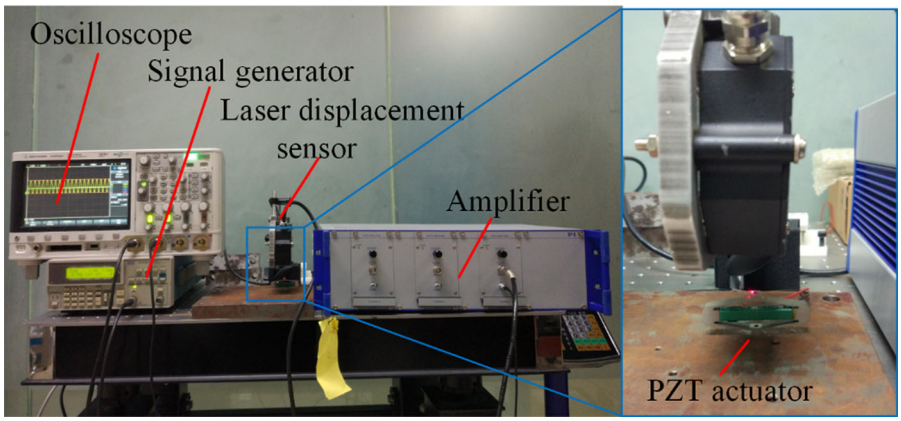

Fig. 3 Experimental platform

In order to obtain the parameters of the established hysteresis model, particle swarm optimization is used to obtain the 10 parameters of the hysteresis model in Eq. (11). And the high-accuracy approximate calculation of G-L definition is employed to carry out the numerical simulation of fractional-order operators.

The root-mean-square (RMS) trajectory tracking error is introduced to be the fitness function of particle swarm optimization for reflecting the modeling deviation, which is given by:

$$e_{\mathrm{RMS}} = \frac{\sqrt{\frac{1}{n}\sum_{k=1}^{n}\left(y_d(k) - y(k)\right)^2}}{\max(y_d(k)) - \min(y_d(k))} \times 100\% \qquad (12)$$

where $y_d(k)$ and $y(k)$ are the experimental displacement and simulated displacement. And n is the number of data for numerical calculation.

For the identification process, sinusoidal input signals and actual displacement response of 100 Hz is employed for the parameter estimation. The coefficients and fractional powers of the model are identified at the same time.

The model identification procedure in time domain is as follows:

Step 1: Getting the data of input signals and actual displacement responses.
Step 2: Selection of the identification parameters and initial conditions.
Step 3: Parameter estimation using the PSO.
Step 4: Verification. If the model is unstable, steps from 2 to 4 are repeated.

The model parameters are obtained as follows: $\alpha_1 = 0.5262$, $\alpha_2 = 1.3604$, $\alpha_3 = 0.5801$, $\alpha_4 = 0.9516$, $\alpha_5 = 0.2433$, $\alpha_6 = 0.5255$, $\alpha_7 = 0.93$, $\alpha_8 = 1.48$, $\alpha_9 = 0.28$, $\alpha_{10} = 1.27$, and the accuracy of the identified fitness function is 1.17%, which is the RMS error. Accordingly, the identified fractional-order model can be obtained as:

$$G(s) = \frac{0.2433s^{1.27} + 0.5255}{0.5262s^{0.93} + 1.3604s^{1.48} + 0.5801s^{0.28} + 0.9516} \qquad (13)$$

The root-mean-square (RMS) trajectory tracking error, Eq. (12), is also introduced to evaluate the performance of the model in the following experimental verification.

3.4 Experimental verifications

The fractional-order model identified with 100 Hz frequency is utilized to verify the hysteresis characteristics under the broadband frequency. The comparison between experimental results and the fractional-order model is shown in Fig. 4. The figure contains the comparison between the time curve and hysteresis loop at 50 Hz, 100 Hz and 200 Hz. The direction hysteresis loops shown in Fig. 4 is anticlockwise. It can be observed from Fig. 4a, b that the model agrees well with the experimental data at 100 Hz and the RMS trajectory tracking error of the model is 1.17%. The experimental data at 200 Hz shown in Fig. 4c, d have the RMS trajectory tracking error of 9.10%, as well as the RMS error 5.98% of 50 Hz shown in Fig. 4e, f. In order to analyze the bandwidth performance of

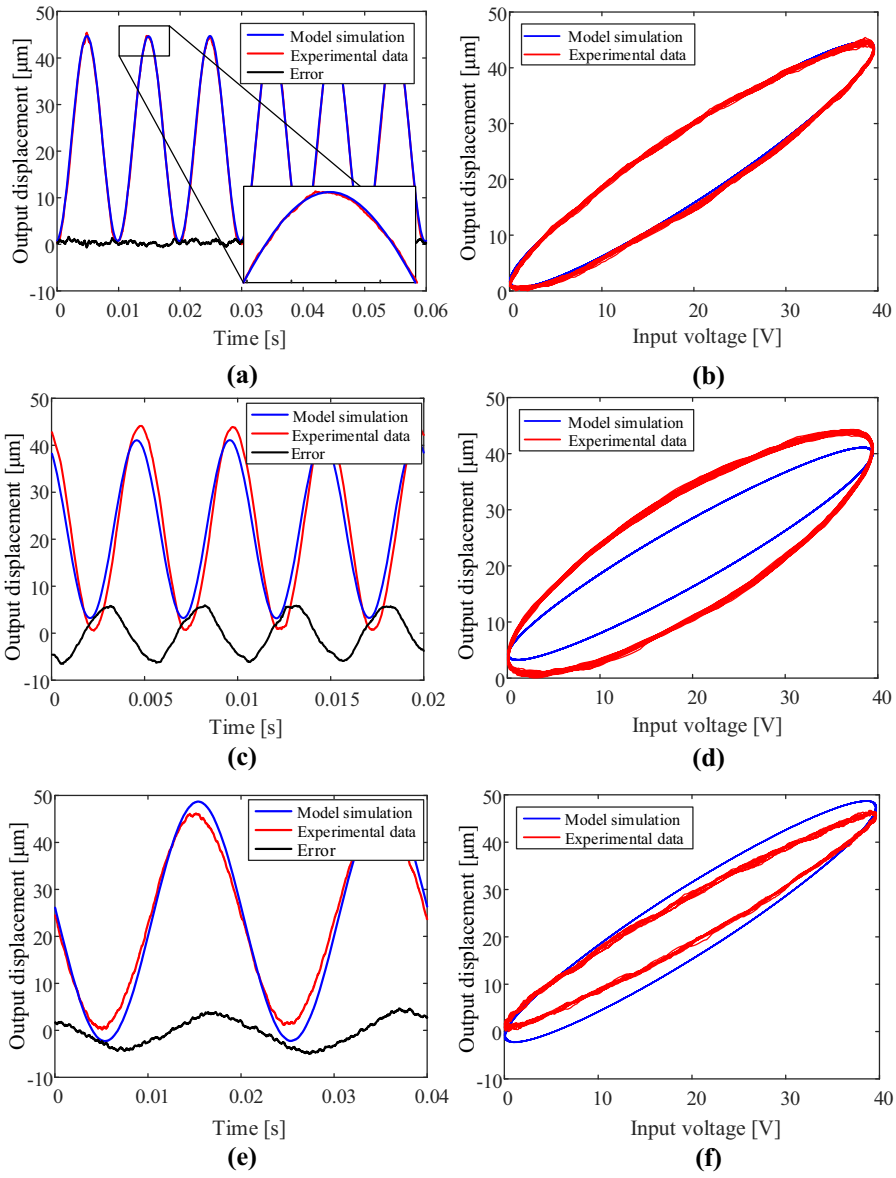

Fig. 4 The comparison between experimental results and the fractional-order model with different frequencies: **a** Time curve at 100 Hz; **b** Hysteresis loop at 100 Hz; **c** Time curve at 200 Hz; **d** Hysteresis loop at 200 Hz; **e** Time curve at 50 Hz; **f** Hysteresis loop at 50 Hz

time domain fractional model, Bode diagram of the identified fractional model is plotted in Fig. 5. It is observed that the model simulation curve only agrees well with experimental data in 100 Hz from the comparison of the fractional-order model and experimental results in Fig. 5. Numerical simulation and experimental results demonstrate the effectiveness of the proposed time domain fractional-order model to describe the nonlinear hysteresis of piezoelectric actuators at a specifically identified frequency while it may not agree well with other frequencies. The identification in the time domain may not be suitable for modeling demands in a wide range of frequencies. In the next section, a modified approach for fractional-order model identification in the frequency domain will be proposed.

4 Hysteresis identification in frequency domain

In this section, to extend the bandwidth of the model established using fractional calculus, a modified approach for parameter identification in the frequency domain is provided.

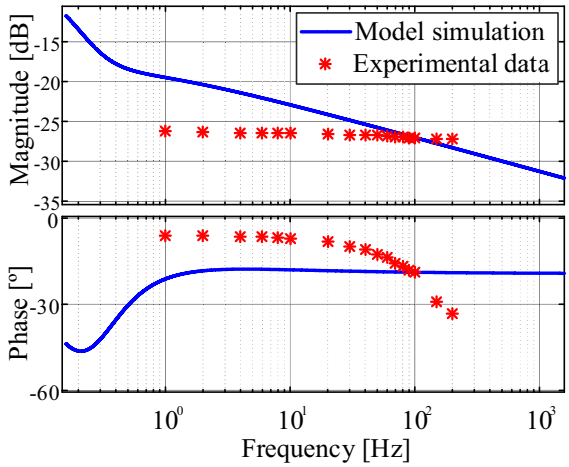

Fig. 5 The comparison of the fractional-order model and experimental results in the Bode diagram

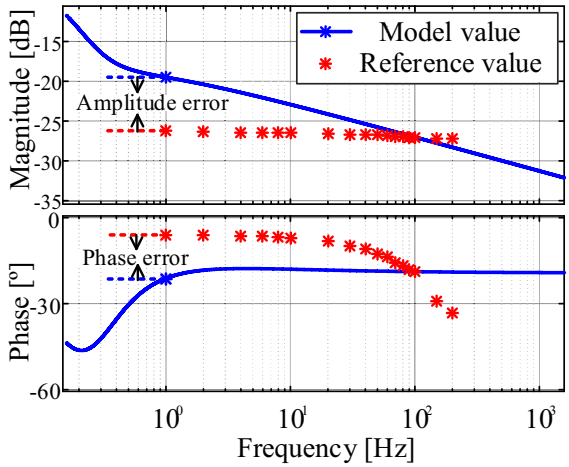

Fig. 6 Schematic diagram of the amplitude error and phase error

4.1 Frequency identification of Hysteresis model

It is mentioned before that the hysteresis error will enlarge and the output amplitude will decrease with the increase in the input signal frequency. Moreover, there are always phase-shift and amplifier modulation in the hysteresis system. Amplitude error is the amplitude difference and the phase error is the phase lag between model value and reference value. The hysteresis model of piezoelectric actuators can be evaluated by the two errors if the reference amplitude and phase values of the PZT hysteresis system are obtained. Figure 6 shows the schematic diagram of the amplitude error and phase error in Bode diagram. And it can be observed that the main differences between the model values and reference values are amplitude and phase errors. If the two errors are reduced in each frequency, the model value and reference value will fit each other well in full span range. Similarly, the model curve will have a good agreement with the reference curve in time domain at each frequency. So the fractional-order hysteresis model can be identified with the changing amplitude and phase values of hysteresis response at different frequencies in frequency domain.

The original changing reference amplitude and phase values can be obtained from the input voltage and output displacement. Then, employing initial calculation to the original values, 17 sets of data of reference amplitude and phase values are obtained with several frequencies. All the real hysteresis values will be used to identify the model in the frequency domain.

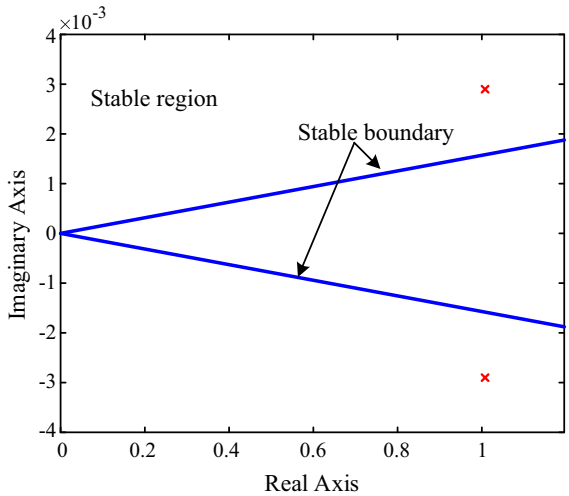

Fig. 7 Pole position and stability region

Multi-tracker Optimization Algorithm (MTOA) [35] is applied to obtain the parameters of the hysteresis model. To have an accurate estimation of the multidimensional minimization problem, the key issue is to find a proper set of parameters to minimize the deviation between modeling curve and experimental reference point in the Bode diagram. Herein, the global maximum error is employed as the fitness function for reflecting the modeling deviation, which is given as:

$$\text{Error}_{\max} = \max\left\{\sqrt{k_i^2 + 1 - 2k_i\cos\phi_i}\right\} \tag{14}$$

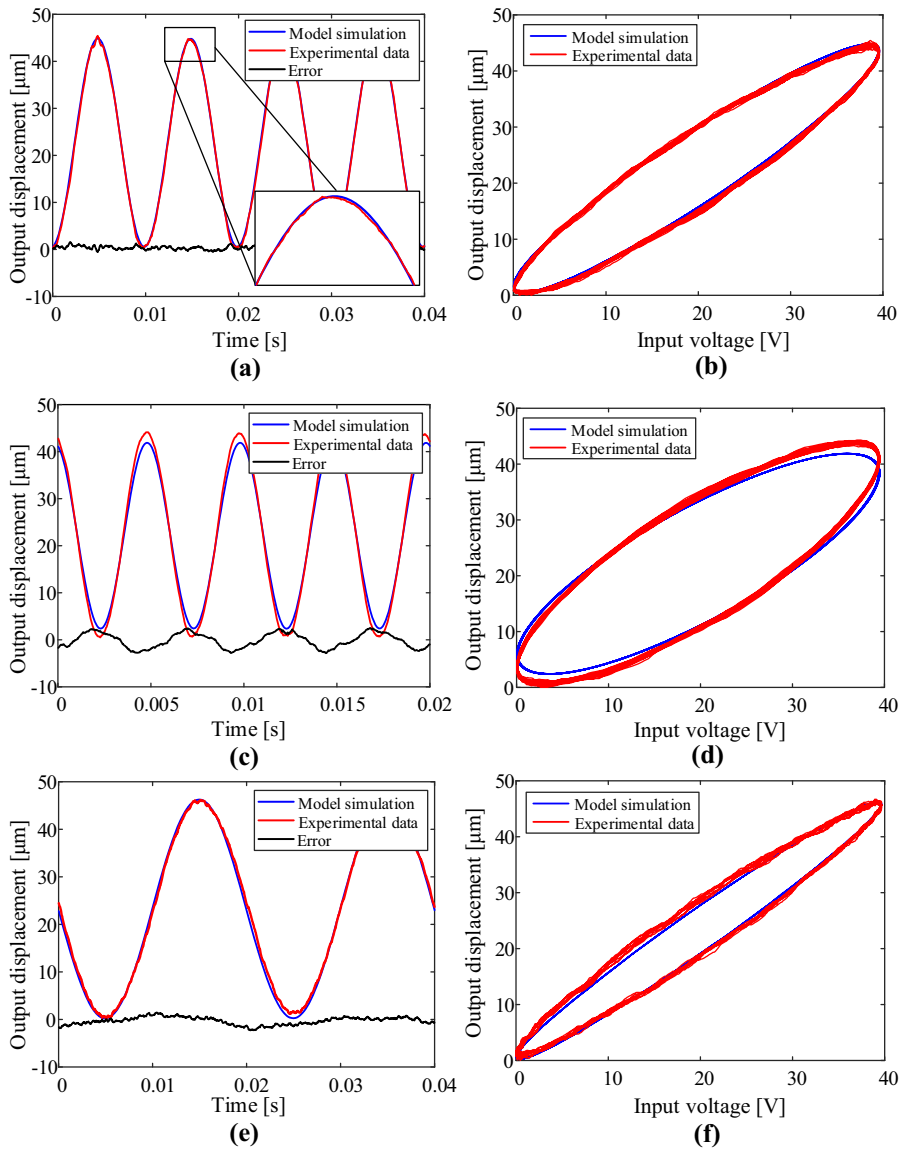

Fig. 8 The comparison of experimental results and the fractional-order model with different frequencies, **a** time curve at 100 Hz; **b** hysteresis loop at 100 Hz; **c** time curve at 200 Hz; **d** hysteresis loop at 200 Hz; **e** time curve at 50 Hz; **f** hysteresis loop at 50 Hz

where k_i is the ratio of the amplitude reference value to the model value; φ_i is the difference between phase reference value and model value.

The coefficients and fractional powers of the model are identified at the same time. And the model identification procedure in frequency domain is as follows:

Step 1: Getting the data of the changing amplitude and phase values in the frequency domain.
Step 2: Selection of the identification parameters and initial conditions.
Step 3: Parameter estimation using the MTOA.
Step 4: Verification. If the model is unstable, steps from 2 to 4 are repeated.

Based on the amplitude and phase information obtained from experimental displacement response under several frequencies, model parameters of Eq. (11) are identified as: $\alpha_1 = 304$, $\alpha_2 = 569324$, $\alpha_3 = 668096$, $\alpha_4 = 292172$, $\alpha_5 = 70714$, $\alpha_6 = 35966$, $\alpha_7 = 1.998$, $\alpha_8 = 0.892$, $\alpha_9 = 0.927$, $\alpha_{10} = 0.875$. And the accuracy of the identified fitness function is 3.76%, which is the global maximum error. Accordingly, the identified fractional-order model can be described as:

$$G(s) = \frac{70714s^{0.875} + 35966}{304s^{1.998} + 569324s^{0.892} + 668096s^{0.927} + 292172} \tag{15}$$

The stability of the model mainly depends on the differential orders, and the stability analysis is employed. The least common divisor of the differential orders is $d = 0.001$. If $\lambda = s^{0.001}$, the pole position plot of λ and the stable boundary can be drawn in Fig. 7. The stability boundary is $d\pi/2 = 0.009°$. It is obvious that all the poles are located in the stable region, which proves that the model is stable.

4.2 Experimental verification and discussion

The model identified in the frequency domain is utilized to verify the hysteresis characteristics under broadband frequency. The comparison between experimental results and the fractional-order model is illustrated in Fig. 8, containing the time curve and hysteresis loop at 50 Hz, 100 Hz and 200 Hz. And the hysteresis loops direction of experimental results and fractional-order model in Fig. 8 is anticlockwise. It can be observed from Fig. 8a, b that the model agrees well with the experimental data at 100 Hz, even in the peak and valley cases; they are fitted well with each other. And the RMS trajectory tracking error of the model is 1.16%. At 200 Hz, it agrees well with the experimental data shown in Fig. 8c, d, and it has the max RMS error in the peak case but no more than 3.53%. There is the RMS error 1.63% of 50 Hz shown in Fig. 8e, f. It can be viewed from Bode diagram shown in Fig. 9 that the identified model has a good agreement with experimental data in the frequency range from 1 to 200 Hz. To study the identification accuracy, the proposed fractional-order models are compared with Bouc–Wen model. Bouc–Wen model is one of the classical models to describe nonlinear hysteresis characters and applied to a wide variety of engineering problems. Table 1 indicates a comparison of the model errors identified in the time domain and frequency domain, as well as Bouc–Wen model. It can be viewed from Table 1 that the presented identified model in frequency domain has better accuracy when compared with Bouc–Wen model in the wider frequency bandwidth. It illustrates that the model identified in the frequency domain performs well in a wider frequency range from 1 to 200 Hz with the maximum modeling error 4.47%. Numerical simulation and experimental results demonstrate the identified fractional-order model in the frequency domain is effective to describe the hysteresis with a wide frequency width. When compared with the proposed frequency domain method, the above time domain identification method in the Sect. 3 has a larger deviation due to that only the input and output response under a constant frequency are employed. On the contrary, all the output response under a certain of wide bandwidth is utilized in the frequency domain.

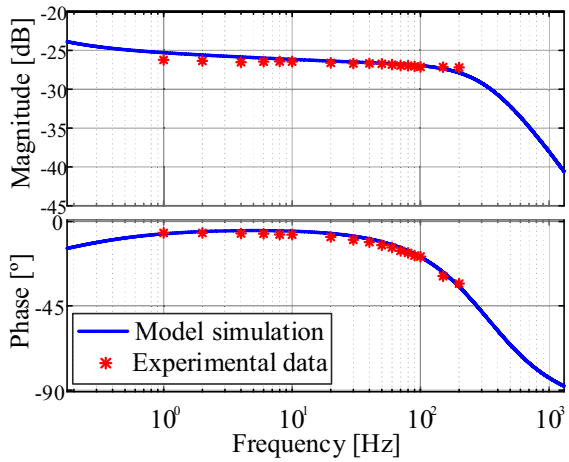

Fig. 9 The comparison between the fractional-order model and experimental results in the Bode diagram

5 Conclusion

In this paper, fractional-order model methods are proposed to describe broadband hysteresis of piezoelectric actuators. The fractional-order model is utilized to describe the relationship between the input voltage and the output displacement of a piezoelectric actuator. An approach is developed to identify the parameters of the fractional-order model. The fractional-order identification methods in the time domain are proposed by using the input voltage and output displacement of the piezoelectric actuator. Moreover, reference amplitude and phase values are employed to identify the fractional model in the frequency domain for improving the model accuracy in a wide bandwidth. Different experiments under time and frequency domain are performed to verify the effectiveness of the proposed methods. The comparison between the identified two models is performed at various frequencies. All results show that the identified model in the frequency domain has a higher

Table 1 The comparison of the model errors

Frequency (Hz)	Model error of Bouc–Wen model (%)	Model error identified in time domain (%)	Model error identified in frequency domain (%)
1	1.57	43.78	4.47
20	2.11	13.72	1.97
30	2.93	9.85	1.57
50	4.73	5.98	1.63
70	6.29	3.15	1.24
100	8.94	1.17	1.16
150	12.94	4.99	1.66
200	17.29	9.10	3.53

prediction accuracy in the frequency bandwidth ranging from 1 to 200 Hz and the maximum error is about 4.47%. The fractional-order model identified in frequency domain will be helpful to precise modeling and controlling compensation of nonlinear rate-dependent hysteresis of piezoelectric actuators.

Acknowledgements This study has been supported by the National Key Research & Development Program of China (Grant No. 2018YFB1306100) and the National Natural Science Foundation of China (Grant Nos. 51575426, 51421004).

Compliance with ethical standards

Conflict of interest The authors declare no conflict of interest.

References

1. Zhang, Z., Yang, X., Yan, P.: Large dynamic range tracking of an XY compliant nanomanipulator with cross-axis coupling reduction. Mech. Syst. Signal. Process. **117**, 757–770 (2019)
2. Liu, Y., Yang, X., Chen, W., Xu, D.: A bonded-type piezoelectric actuator using the first and second bending vibration modes. IEEE. T. Ind. Electron. **63**(3), 1676–1683 (2016)
3. Ling, M., Cao, J., Jiang, Z., Lin, J.: Modular kinematics and statics modeling for precision positioning stage. Mech. Mach. Theory. **107**, 274–282 (2017)
4. Orszulik, R.R., Shan, J.: Output feedback integral control of piezoelectric actuators considering hysteresis. Precis. Eng. **47**, 90–96 (2017)
5. Ling, M., Cao, J., Zeng, M., Lin, J., Inman, D.J.: Enhanced mathematical modeling of the displacement amplification ratio for piezoelectric compliant mechanisms. Smart. Mater. Struct. **25**(7), 075022 (2016)
6. Ji, D.H., Koo, J.H., Yoo, W.J., Ju, H.P.: Precise tracking control of piezoelectric actuators based on a hysteresis observer. Nonlinear Dyn. **70**(3), 1969–1976 (2012)
7. Qi, C., Gao, F., Li, H.X., Li, S., Zhao, X., Dong, Y.: An incremental Hammerstein-like modeling approach for the decoupled creep, vibration and hysteresis dynamics of piezoelectric actuator. Nonlinear Dyn. **82**(4), 1–22 (2015)
8. Gu, G.Y., Yang, M.J., Zhu, L.M.: Real-time inverse hysteresis compensation of piezoelectric actuators with a modified Prandtl–Ishlinskii model. Rev. Sci. Instrum. **83**(6), 65–83 (2012)
9. Ge, P., Jouaneh, M.: Modeling hysteresis in piezoceramic actuators. Precis. Eng. **17**(3), 211–221 (1995)
10. Tang, H., Li, Y.: Feedforward nonlinear PID control of a novel micromanipulator using Preisach hysteresis compensator. Robot. Cim Int. Manuf. **34**, 124–132 (2015)
11. Li, Z., Zhang, X., Su, C.Y., Chai, T.: Nonlinear control of systems preceded by preisach hysteresis description: a prescribed adaptive control approach. IEEE. Trans. Contr. Syst. T. **24**(2), 451–460 (2016)
12. Yang, M.J., Gu, G.Y., Zhu, L.M.: Parameter identification of the generalized Prandtl–Ishlinskii model for piezoelectric actuators using modified particle swarm optimization. Sens. Actuat. A Phys. **189**(2), 254–265 (2013)
13. Gu, G.Y., Zhu, L.M., Su, C.Y.: Modeling and compensation of asymmetric hysteresis nonlinearity for piezoceramic actuators with a modified Prandtl–Ishlinskii model. IEEE. Trans. Ind. Electron. **61**(3), 1583–1595 (2014)
14. Janaideh, M.A., Krejci, P.: Inverse rate-dependent Prandtl–Ishlinskii model for feedforward compensation of hysteresis in a piezomicropositioning actuator. IEEE ASME Trans. Mech. **18**(5), 1498–1507 (2013)
15. Qin, Y., Tian, Y., Zhang, D., Shirinzadeh, B., Fatikow, S.: A novel direct inverse modeling approach for hysteresis compensation of piezoelectric actuator in feedforward applications. IEEE ASME Trans. Mech. **18**(3), 981–989 (2013)
16. Rakotondrabe, M.: Multivariable classical Prandtl–Ishlinskii hysteresis modeling and compensation and sensorless control of a nonlinear 2-dof piezoactuator. Nonlinear Dyn. **89**(1), 1–19 (2017)
17. Liu, Y., Shan, J., Gabbert, U., Qi, N.: Hysteresis and creep modeling and compensation for a piezoelectric actuator using a fractional-order Maxwell resistive capacitor approach. Smart Mater. Struct. **22**(11), 5020 (2013)

18. Liu, Y., Shan, J., Gabbert, U., Qi, N.: Hysteresis compensation and trajectory preshaping for piezoactuators in scanning applications. Smart Mater. Struct. **23**(1), 015015 (2014)
19. Shan, J., Liu, Y., Gabbert, U., Cui, N.: Control system design for nano-positioning using piezoelectric actuators. Smart Mater. Struct. **25**(2), 025024 (2016)
20. Bouc, R.: A mathematical model for hysteresis. Acta. Acust. United Ac **24**(1), 16–25(10) (1971)
21. Wang, D.H., Zhu, W., Yang, Q.: Linearization of stack piezoelectric ceramic actuators based on Bouc–Wen model. J. Intel. Mat. Syst. Str. **22**(5), 401–413 (2010)
22. Wang, Z.Y., Mao, J.Q.: On PSO Based Bouc–Wen modeling for piezoelectric actuator. In: International Conference, pp. 125–134 (2010)
23. Chen, Y.Q., Xue, D., Dou, H.: Fractional calculus and biomimetic control. In: IEEE International Conference on Robotics and Biomimetics, pp. 901–906 (2005)
24. Chen, Y.Q.: Ubiquitous fractional order controls? IFAC Proc. Vol. **39**(11), 481–492 (2010)
25. Zhou, S., Cao, J., Chen, Y.: Genetic algorithm-based identification of fractional-order systems. Entropy **15**(5), 1624–1642 (2013)
26. Danca, M.F., FecKan, M., Kuznetsov, N.V., Chen, G.: Fractional-order PWC systems without zero Lyapunov exponents. Nonlinear Dyn. **91**(4), 2523–2540 (2018)
27. Fan, Y., Xia, H., Zhen, W., Li, Y.: Nonlinear dynamics and chaos in a simplified memristor-based fractional-order neural network with discontinuous memductance function. Nonlinear Dyn. **9**, 1–17 (2018)
28. Wang, L., Cheng, P., Wang, Y.: Frequency domain subspace identification of commensurate fractional order input time delay systems. Int. J. Control Autom. **9**(2), 310–316 (2011)
29. Liu, Y., Liu, H., Zhu, D.: Modeling, identification, and compensation of fractional-order creep in frequency domain for piezoactuators. Electron. Lett. **52**(17), 1444–1445 (2016)
30. Zakeri, E., Moezi, S., Eghtesad, M.: Optimal interval type-2 fuzzy fractional order super twisting algorithm: a second order sliding mode controller for fully-actuated and under-actuated nonlinear systems. ISA Trans. **85**, 13–32 (2018)
31. Zolotas, A.C., Goodall, R.M.: New insights from fractional order skyhook damping control for railway vehicles. Veh. Syst. Dyn. **56**(11), 1658–1681 (2018)
32. Rebai, A., Guesmi, K., Gozim, D., Hemici, B.: Identification of the PEA hysteresis property using a fractional order model. In: International Conference on Sciences and Techniques of Automatic Control and Computer Engineering, pp. 1038–1043 (2015)
33. Li, L.L., Gu, G.Y., Zhu, L.M.: A fractional-order active damping control approach for piezo-actuated nanopositioning stages. In: International Conference on Manipulation, Automation and Robotics at Small Scales, pp. 1–6 (2016)
34. Liu, Y., Shan, J., Gabbert, U., Qi, N.: Hysteresis and creep modeling and compensation for a piezoelectric actuator using a fractional-order Maxwell resistive capacitor approach. Smart Mater. Struct. **22**(11), 115020 (2013)
35. Zakeri, E., Moezi, S.A., Bazargan-Lari, Y., Zare, A.: Multi-tracker optimization algorithm: a general algorithm for solving engineering optimization problems. Iran J. Sci. Technol. Trans. Mech. Eng. **41**(4), 315–341 (2017)